

Control of flow over a cylinder using rotational oscillations

Prasenjit Ray, Panagiotis D. Christofides*

Department of Chemical Engineering, University of California, 405 Hilgard Avenue, Box 951592, Los Angeles, CA 90095-1592, USA

Available online 11 November 2004

Abstract

In this work, we focus on two-dimensional, incompressible viscous channel flow over an infinitely long cylinder and examine the effect of controlled rotational cylinder oscillation in reducing the drag exerted on the cylinder. Based on an analysis of the open-loop simulations, a control system is designed that automatically determines the frequency of cylinder oscillation, based on the Reynolds number, to consistently reduce the drag exerted on the cylinder for Reynolds numbers in the range 100–500.

© 2004 Elsevier Ltd. All rights reserved.

Keywords: Flow over a circular cylinder; Rotational oscillation; Active feedback control

1. Introduction

Control of flow past a circular cylinder is studied for a number of practical reasons. Wake modification, reduction of flow-induced vibrations, design of heat exchangers, and improvement of chemical mixing are among the diverse applications involving flow past a circular cylinder. This problem is also studied for stall control and lift enhancement as well as for design of aerodynamic vehicles.

The formation of vortices behind the flow past a circular cylinder above a critical Reynolds number has been well documented, both numerically and experimentally (e.g., Batchelor, 1967; Li, Chambarel, Donneaud, & Martin, 1991; Lu & Sato, 1996; Shiels & Leonard, 2001; Taneda, 1977; Tokumaru & Dimotakis, 1991; Williamson, 1996). Initially, at flows below Reynolds number 10, the fluid travels along the boundary of the cylinder and streamlines form around the cylinder. At Reynolds number above roughly 10, the streamlines separate from the boundary behind the cylinder and vortices are formed. These vortices remain behind the cylinder. At Reynolds number above roughly 47, these vortices are successively formed and then shed from the top and bottom of the cylinder periodically. The regular pattern of shedding vortices is called the von Karman vortex street (Batchelor,

1967). The reader may refer to (Williamson, 1988, 1996) for detailed studies of the behavior of cylinder wakes, especially focusing on the relationship between vortex shedding frequency and Reynolds number.

The effective control of drag exerted by the fluid on the cylinder has been a challenge that has received particular attention. The drag force on the cylinder may be reduced by active control in the form of cylinder rotational oscillation. Taneda (1977) made early visual observations and studied the behavior of the wake of several different bluff bodies. In this work, the effect of a number of different kinds of unsteady motions was studied, including impulsive start from rest, change of velocity, and rotational oscillation. While providing detailed observations of wake structures and observing boundary layer development, this work did not consider a range of rotational oscillation conditions (varying amplitude and frequency of rotation) and did not carry out drag measurements on the circular cylinder undergoing rotational oscillation. Tokumaru & Dimotakis (1991); conducted experiments on flow past a cylinder at Reynolds number 15,000 for a variety of amplitudes and frequencies of oscillation, finding that significant drag reduction was possible with active control. In this work, the effects of multiple forcing conditions are considered in detail, however, essentially all of this study is performed at Reynolds number 15,000 and the effects of active control at a range of different Reynolds numbers is not investigated. The control methodology proposed in Toku-

* Corresponding author. Tel.: +1 310 794 1015; fax: +1 310 206 4107.

E-mail address: pdc@seas.ucla.edu (Panagiotis D. Christofides).

maru et al. is open-loop and, therefore, does not involve any elements of feedback or feedforward control (Tokumaru & Dimotakis, 1991). Shiels and Leonard (2001) carried out numerical studies to complement Tokumaru's work; see also (Lu & Sato, 1996; Protas & Wesfreid, 2002) for further parametric studies.

Studies have also been conducted on closed-loop control of the circular cylinder wake. Roussopoulos (1993) conducted an experimental study where the wake of a circular cylinder in low Reynolds number flow was stabilized by feeding back velocity data from the flow field behind the cylinder using acoustic actuation. Singh, Myatt, Addington, Banda and Hall, 2001 used linear optimal control theory to control a reduced-order cylinder flow model that was constructed by applying proper orthogonal decomposition (POD) to flow field data, see also (Armaou & Christofides, 2000a, 2000b; Baker, Armaou, & Christofides, 2002; Baker & Christofides, 2002; Christofides & Armaou, 2000) for further results on linear/nonlinear feedback control of fluid dynamic systems using reduced-order models and (Aamo & Krstić, 2003) for a recent review of results on feedback control of fluid flows). Gillies (2001) used multiple sensors to control the one-dimensional Ginzburg–Landau equation, which is a PDE model that captures some of the stability features of the two-dimensional cylinder wake. Park, Ladd, and Hendricks (1993) used blowing/suction actuation on the one-dimensional Ginzburg–Landau equation and examined the effect of sensor location on the performance of the feedback controller.

The present work focuses on two-dimensional, incompressible viscous channel flow over an infinitely long cylinder and examines the effect of controlled rotational cylinder oscillation in reducing the drag exerted on the cylinder. Initially, a description of the flow field and of the governing equations is given together with a precise specification of the drag exerted on the cylinder. Then, the solution of the flow field for the stationary cylinder is given and the drag on the cylinder is validated against available numerical studies. The effect of controlled cylinder oscillation in reducing the drag exerted on the cylinder is subsequently examined. Based on an analysis of the open-loop simulations, a control system is designed that automatically determines the frequency of cylinder oscillation, based on the Reynolds number, to consistently reduce the drag exerted on the cylinder for Reynolds numbers in the range 100–500.

2. Flow field: description and governing equations

We consider a two-dimensional incompressible, viscous channel flow past a cylinder. A schematic of the flow field is given in Fig. 1. The incompressible Navier–Stokes equations are used to describe the flow field. In two dimensions, the dimensionless Navier–Stokes equations take the following form:

$$\begin{aligned} \frac{\partial u}{\partial x} + \frac{\partial v}{\partial y} &= 0 \\ \frac{\partial u}{\partial t} + u \frac{\partial u}{\partial x} + v \frac{\partial u}{\partial y} &= -\frac{\partial p}{\partial x} + \frac{1}{Re} \left(\frac{\partial^2 u}{\partial x^2} + \frac{\partial^2 u}{\partial y^2} \right) \\ \frac{\partial v}{\partial t} + u \frac{\partial v}{\partial x} + v \frac{\partial v}{\partial y} &= -\frac{\partial p}{\partial y} + \frac{1}{Re} \left(\frac{\partial^2 v}{\partial x^2} + \frac{\partial^2 v}{\partial y^2} \right) \end{aligned} \quad (1)$$

where u and v are the components of the velocity along the x (parallel to the channel wall) and y (normal to the channel wall) axes, respectively, and p is the pressure. The Reynolds number is defined as $Re = (U_{\text{mean}}d/\nu)$ where U_{mean} is the mean velocity in the channel, d is the diameter of the cylinder and ν is the kinematic viscosity. Eq. (1) is subjected to the following no-slip, no-penetration boundary conditions at the top and bottom walls of the channel:

$$\begin{aligned} u(x, y = 0, t) &= u(x, y = 1, t) = 0 \\ v(x, y = 0, t) &= v(x, y = 1, t) = 0 \end{aligned} \quad (2)$$

The lack of knowledge of the flow field at the outlet boundary of the spatial domain prohibits the use of traditional boundary conditions, such as assuming zero total force or axial force, or assuming some fully developed profile (Papanastasiou, Malamataris & Ellwood, 1992). Motivated by this, the so-called free boundary condition is employed at the outlet boundary (Papanastasiou et al., 1992; Renardy, 1997) (see also Baker, Myatt, & Christofides, 2002 for an implementation of this boundary condition in flow over a flat plate). The solution of the flow field with the free boundary condition can be accomplished by determining the surface and volume integrals from the residuals of the Navier–Stokes equations formed during discretization. According to the free boundary condition, the pressure is specified as a constant at the outlet boundary (Papanastasiou et al., 1992; Renardy, 1997):

$$p(x = 1, y, t) = 0 \quad (3)$$

For stationary cylinder simulations, the boundary of the cylinder is subjected to the same no-slip, no-penetration boundary

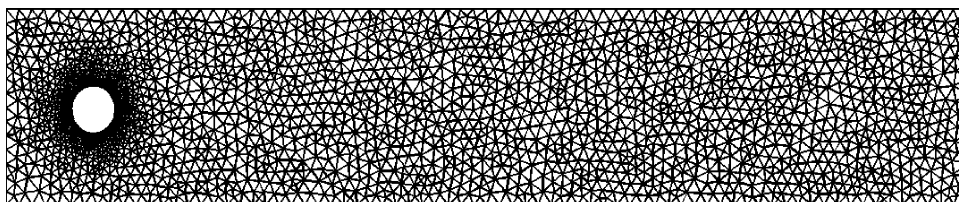


Fig. 1. Schematic of the spatial domain of the flow field and structure of the finite element mesh.

conditions of the type of Eq. (2). The inlet boundary condition is specified as follows:

$$\begin{aligned} u(x=0, y, t) &= 4U_{\max}y(1-y) \\ v(x=0, y, t) &= 0 \end{aligned} \quad (4)$$

where U_{\max} is the maximum incoming velocity in the center of the channel.

To simulate a rotating cylinder, the no-slip boundary conditions used for the stationary cylinder are modified. The cylinder is subjected to periodically oscillating boundary conditions, described by the following equations:

$$\begin{aligned} u &= yA \sin(2\pi f_f t) \\ v &= -xA \sin(2\pi f_f t) \end{aligned} \quad (5)$$

These boundary conditions result in an overall rotation of the cylinder with amplitude A and forcing frequency f_f .

The equations that describe the flow field are solved within the FEMLAB simulation environment (COMSOL Incorporated, 2001) that uses a finite element approach to compute the solution of the flow field. The structure of the finite element mesh used in our calculations is shown in Fig. 1. The region of the flow field with the largest temporal and spatial gradients is around and directly behind the cylinder, therefore, the mesh is very well refined around the cylinder edges. To reduce the computational load, the mesh is less refined further away from the cylinder, where the temporal and spatial gradients are smaller. Further increase in the number of elements and decrease of the step size of the temporal integration did not influence the accuracy of the computed results.

At Reynolds number 100, vortices are shed regularly at a frequency f which has different values for various geometries. To facilitate comparison of results obtained for different flow fields, the dimensionless frequency, the Strouhal number, St , is defined by the following relationship:

$$St = \frac{fd}{U_{\text{mean}}} \quad (6)$$

The natural Strouhal number, St_{nat} , is obtained by using the natural vortex shedding frequency, f_{nat} , for f in Eq. (6) (Shiels & Leonard, 2001).

A cylinder moving through a fluid experiences a drag force, F_D , in the direction parallel to the flow. This force has two components: the frictional (or viscous) drag, F_{frict} , and the pressure (or form) drag, F_{press} (Batchelor, 1967; Juárez, Scott, Metcalfe, & Bagheri, 2000). The frictional drag is caused by the formation of the boundary layer on the surface, while pressure drag is attributed to the formation of the wake behind the cylinder. The pressure drag, F_{press} , is the component of pressure that is normal to the surface of the cylinder, and the frictional drag, F_{frict} , is the tangential component of the shear stress. The total drag, F_D , is defined by (Batchelor, 1967; Juárez et al., 2000):

$$F_D = \int_{\Gamma} (-P\mathbf{n} + \boldsymbol{\tau} \cdot \mathbf{n})(s) \cdot \mathbf{e}_x \, ds \quad (7)$$

where P is the pressure, \mathbf{n} the unit outward normal vector at the boundary, $\boldsymbol{\tau}$ the viscous stress tensor defined at a generic point s taken on the boundary Γ of the cylinder, and \mathbf{e}_x the unit vector in the x coordinate direction. The first term of the integral is F_{press} , and the second term is the contribution from F_{frict} . The objective of implementing active control in this problem is to reduce the overall drag experienced by the cylinder using rotational oscillation. The dimensionless drag coefficient (per unit length) is defined by the following expression (Batchelor, 1967):

$$C_D = \frac{F_D}{1/2(\rho U_{\text{mean}}^2 d)} \quad (8)$$

where F_D is the total drag force on the cylinder as defined in Eq. (7), ρ is the density of the fluid, which is unity in our simulations, and d is the diameter of the cylinder.

3. Solution of the flow field

In this section, we present representative results of our simulations and compare with existing results (further details of our study can be found in (Ray, 2003)). Specifically, in a study to compare different solution methods, Schäfer (Schäfer & Turek, 1996) compared the results of 15 different groups that were tasked to solve the flow problem considered in this work at Reynolds numbers 20 and 100; we compare our results with (Schäfer & Turek, 1996).

The profile of the flow field at Reynolds number 20 is shown in Fig. 2. Vortices are formed behind the cylinder at this Reynolds number but remain attached to the cylinder and are not shed into the flow field; the drag on the cylinder remains constant over time. The resulting C_D is 5.58 which compares very well with the C_D computed by the groups in Schäfer's study which was between 5.57 and 5.59 (Schäfer & Turek, 1996).

At Reynolds numbers above the critical value of roughly 47, vortex shedding from the cylinder occurs. This vortex shedding results in fluctuations of the drag force on the cylinder. Vortices are shed from alternate sides of the cylinder. As each vortex is shed, a force is applied to each side of the cylinder and the overall mean drag fluctuates (see Fig. 3). Solutions of the flow field at Reynolds number 100 are also summarized in Schäfer & Turek (1996). A total of ten different approaches were used. Based on these results, the maximum C_D was between 3.22 and 3.24 (Schäfer & Turek, 1996). For the present study, the resulting maximum drag coefficient was found to be 3.22. The variation of drag coefficient over time is shown in Fig. 3.

After the maximum drag is reached, the value of C_D exhibits small oscillations around its mean value, 3.17. The velocity field after 10 s at Reynolds number 100 is shown in Fig. 4. At Reynolds numbers greater than a critical value, in incompressible, viscous flow, vortices develop in the wake behind the cylinder and are shed into the passing fluid. The shed vortices form a periodic pattern known as the

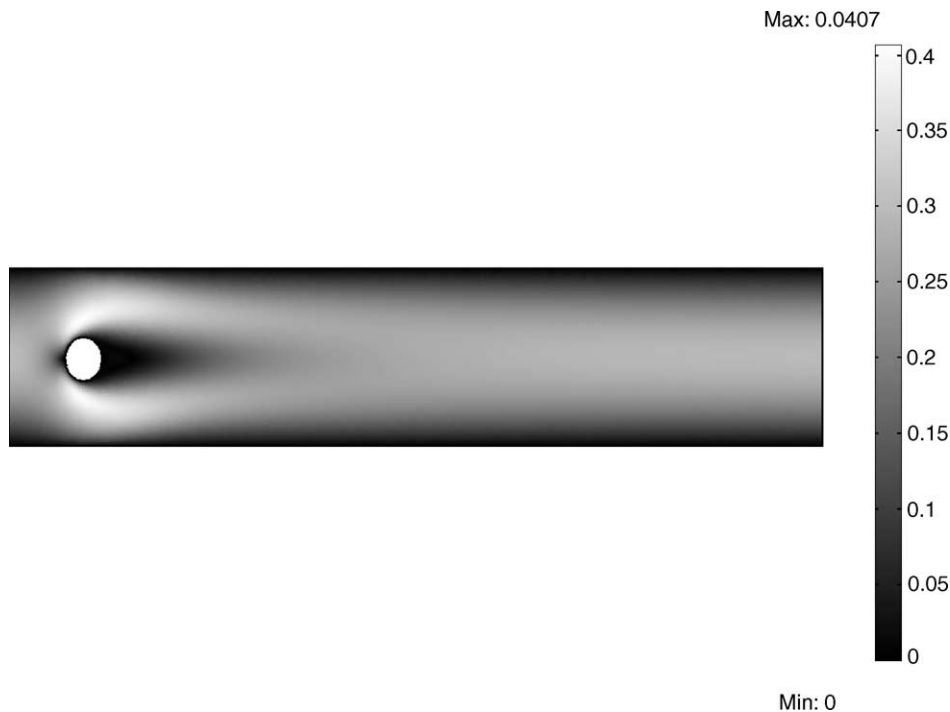


Fig. 2. Velocity field for $Re = 20$ after 10 s.

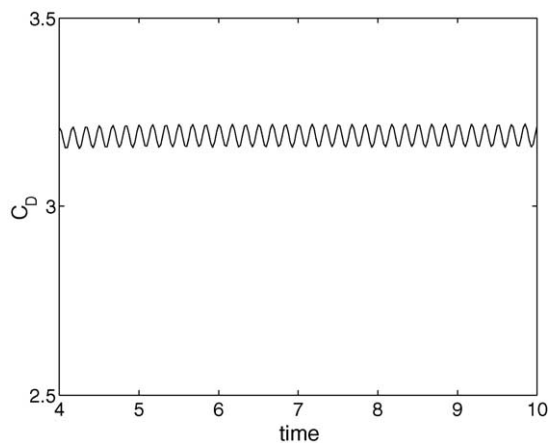


Fig. 3. Change in drag vs. time for $Re = 100$.

von Karman vortex street (Batchelor, 1967). According to Williamson (1996), the critical Reynolds number is 49, while Li et al. (Li et al., 1991) cite a range of 35–47 from a few different researchers. In our study, the critical Reynolds number was found to be around 47.

At a given Reynolds number, the vortices are shed from the cylinder at characteristic natural frequency, f_{nat} , corresponding to a dimensionless frequency called the Strouhal number, $St_{\text{nat}} = f_{\text{nat}} d/U_{\text{mean}}$. For our problem, f_{nat} at Reynolds number 100 is determined to be 3.0, which corresponds to $St_{\text{nat}} = 0.30$. The frequency of vortex shedding varies linearly with Reynolds number in the range 50–500, as shown in Fig. 5; this result is in very good agreement with the results in (Williamson, 1988, 1996).

As discussed above, the total drag force, F_{D} , consists of two components: the pressure drag, F_{press} , and the friction drag, F_{frict} . For a bluff body at low Reynolds number such as the circular cylinder studied in the present work, the majority of the drag force comes from the pressure drag. Protas and Wesfreid (2002) found that, at Reynolds number 150 for the circular cylinder, F_{press} constitutes roughly 81% of the total drag. This value was in agreement with that found in the present study, 81%, for $Re = 150$. Moreover, as the Reynolds number increases, the fractional contribution of F_{press} increases (Ray, 2003).

We now turn to the case of flow past a rotationally oscillating cylinder. There are three main parameters which may be varied for uniform flow past a rotationally oscillating cylinder: Reynolds number, $Re = U_{\text{mean}} d/\nu$, forcing Strouhal number, $St_{\text{f}} = f_{\text{f}} d/U_{\text{mean}}$ (where f_{f} is the forcing frequency), and A , the amplitude of rotation (Lu & Sato, 1996). For compactness, we present our results in terms of $R_{f/n} = St_{\text{f}}/St_{\text{nat}}$, the ratio of the forcing Strouhal number to the natural Strouhal number, and $W = A d/2U_{\text{mean}}$, the normalized amplitude. For Reynolds number 100, Fig. 6 shows C_{D} versus $R_{f/n}$ for varying values of W . At the largest values of W , C_{D} changes very rapidly at values of $R_{f/n}$ below 2. Small values of W result in large values of drag at low frequencies. As $R_{f/n}$ increases, the rate of change of C_{D} decreases. At $R_{f/n} = 5$, very little change in C_{D} is seen even when W is increased by a factor of six. The natural drag was doubled at $R_{f/n} = 1$, followed by a sharp decrease and a very low C_{D} at $R_{f/n} = 5$. This plot shows that a cylinder oscillating at five times St_{nat} exhibits a reduction in C_{D} compared to a stationary cylinder (compare with Fig. 3); this conclu-

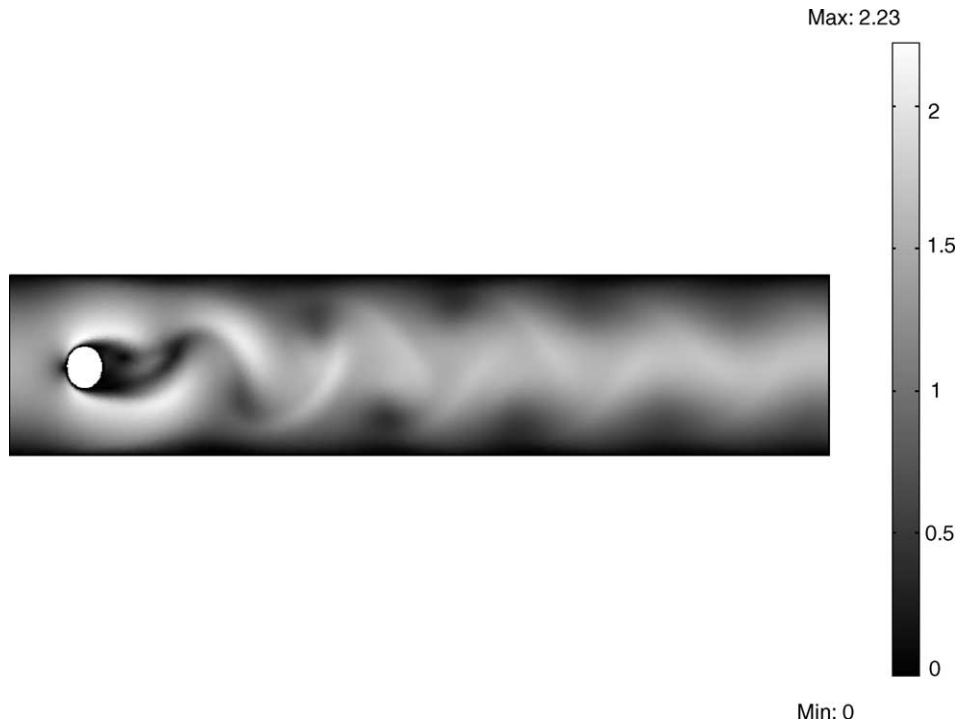


Fig. 4. Velocity field for $Re = 100$ after 10 s.

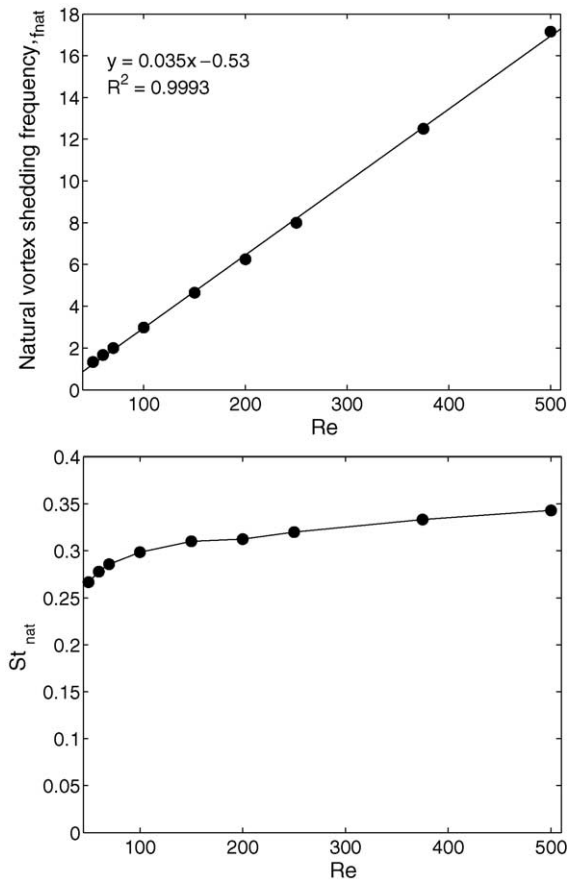


Fig. 5. Relationship between vortex shedding and Re . Top plot: frequency; bottom plot: Strouhal number.

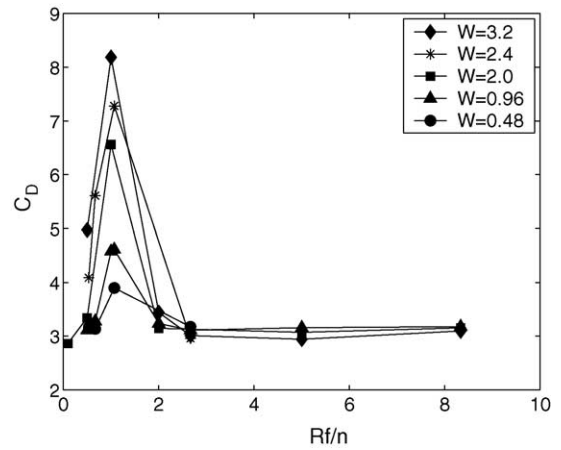


Fig. 6. C_D vs. Rf/n for varying values of $W - Re = 100$.

sion was also drawn for several other Reynolds numbers in the range 100–500. The relationship between C_D and W is shown in Fig. 7 for multiple values of Rf/n .

4. Active control

The present study, among others (Lu & Sato, 1996; Protas & Wesfreid, 2002; Shiels & Leonard, 2001; Tokumaru & Dimotakis, 1991), has shown that a cylinder oscillating at five times St_{nat} exhibits a reduction in C_D compared to a stationary cylinder for Reynolds numbers in the range 100–500. Motivated by this, a control system is developed which senses the

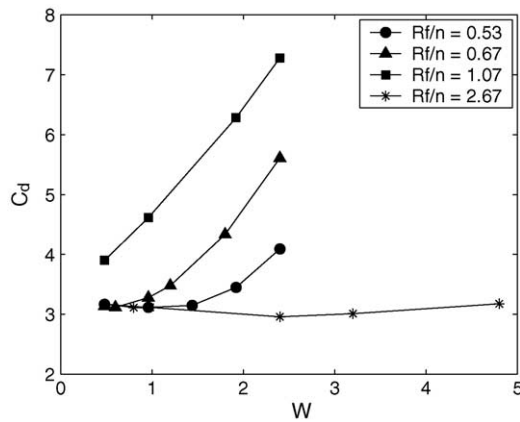


Fig. 7. C_D vs. W for varying values of R_f/n .

speed of the flow field and determines appropriate oscillation parameters based on the Reynolds number. Specifically, an almost linear relationship exists (see Fig. 5) between the natural frequency of vortex shedding, f_{nat} , and the Reynolds number of the flow field in the range 50–500. Using this linear relationship, the $St_f (= (f_f d/U_{mean}) = 5St_{nat})$ was determined for each of the following five Reynolds numbers: 100, 150, 200, 250, and 500. Based on this, a controller was designed which computes the value of the oscillation frequency of the cylinder, f_f , for each Reynolds number using the relationship $f_f = 5(0.035 Re - 0.53)$ for Re in the range 50–500.

To evaluate the performance of this controller, we run several simulations. Specifically, the Reynolds number is increased from 100 to 500. Fig. 8 shows the values of C_D vs. time for two different cases: one open-loop simulation and one closed-loop simulation. Fig. 8 shows only the change from Reynolds number 100–250 in each case. Initially, in both cases, the Reynolds number is 100. After 10 s, the Reynolds number is gradually increased (over a period of 4 s) from 100 to 150. This is accomplished by raising the average flow speed at the inlet boundary, U_{mean} . After the

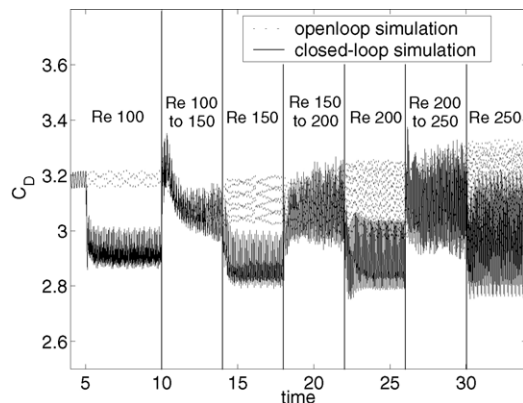


Fig. 8. Closed-loop feedback control: C_D vs. time for Reynolds number varying from 100 to 250 under open-loop (dashed line) and closed-loop (solid line) conditions.

flow is brought to Reynolds number 150, it is held there for another 4 s. In this manner, the Reynolds number is raised over 4 s and successively held for 4 s at 200, 250, and 500. In the closed-loop simulation, the controller is turned on at 5 s at Reynolds number 100. Using the linear relationship given in Fig. 5, the frequency of oscillation is determined by measuring the Reynolds number every 0.01 s and altering the frequency of rotation at the cylinder boundary accordingly. During the periods where the Reynolds number is gradually increased, the frequency of oscillation is also gradually increased, as the controller takes Reynolds number readings every 0.01 s and adjusts the frequency of rotation based on its measurements.

One way to evaluate the performance of the controller is to compare the effect of each of the five frequencies used in the controller at all five of the Reynolds numbers that were considered. Table 1 shows the reduction of C_D at each combination of frequency and Reynolds number. The boldface values are the percent reduction of C_D achieved by oscillating the cylinder at a forcing frequency specified by the controller for the specific Reynolds number.

In most cases, the reductions of C_D resulting from the frequencies specified by the controller are above average compared to the other frequencies tested. For example, for $Re = 100$ the improvement in C_D achieved using the controller (7.49% reduction) is significantly better than that achieved by using all other forcing frequencies (note that the minus sign corresponds to a drag increase compared to the drag under stationary cylinder for the same Reynolds number). The results of Table 1 also emphasize the fact that the proposed controller is not an optimal one, i.e., producing the greatest possible reduction in drag for any given Reynolds number. Rather, the proposed controller produces a consistent drag reduction at a broad range of flow speeds; this is important given the difficulty to determine the appropriate frequency of cylinder oscillation that decreases the drag exerted on the cylinder, for a given Reynolds number, without extensive numerical simulation.

The performance of the controller in the presence of measurement errors was also evaluated. The simulation described above, where the Reynolds number is increased from 100 to 500 (holding the Reynolds number constant at each intermediate Reynolds number for 4 s) is repeated in the presence of measurement errors.

Two cases with measurement errors are simulated. The first case corresponds to underestimation of the sensed flow speed. Specifically, the controller uses 80% of the actual Reynolds number value to determine the forcing frequency. For example, when the flow field is at Reynolds number 100, the controller uses a reading of Reynolds number 80 (instead of the real value of 100), and it then adjusts the frequency of rotation as if the Reynolds number is actually 80. This –20% error is maintained throughout the simulation so that, at every Reynolds number, the controller uses a Reynolds number that is 20% less than the actual. As can be seen in Fig. 9, even with the presence of the measurement error, the controller is

Table 1
Percent reduction of C_D by rotating the cylinder with different f_f for Reynolds numbers in the range 100–500

Re	Forcing frequency, f_f					Nominal C_D
	15	23.256	31.25	40	85	
100	7.49	−2.08	−5.32	−4.01	0.00	3.19
150	16.32	8.78	6.21	2.82	0.18	3.11
200	16.35	11.14	6.14	7.63	0.45	3.11
250	10.37	0.45	7.31	5.04	0.85	3.12
500	−12.04	3.35	−1.90	1.97	1.15	3.13

With bold face letters, we show the reduction achieved by using a forcing frequency specified by the controller for a specific Reynolds number. The minus sign corresponds to a drag increase compared to the drag under stationary cylinder for the same Reynolds number.

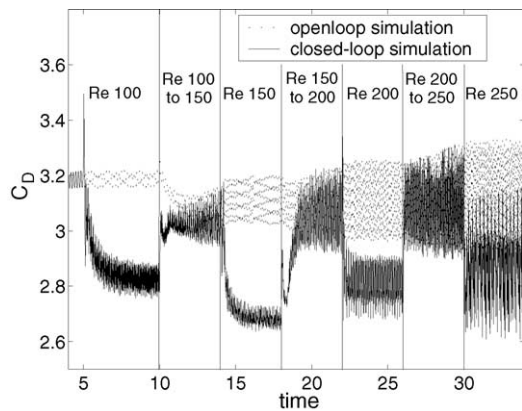


Fig. 9. Closed-loop simulation in the presence of measurement errors: C_D vs. time for Reynolds number varying from 100 to 250 under open-loop conditions (dashed line) and under closed-loop conditions in the presence of -20% measurement error (solid line).

successful at reducing the drag compared to the open-loop case.

The second case with measurement error corresponds to the overestimation of the sensed flow speed. In this case, the controller uses 120% of the actual Reynolds number value to determine the forcing frequency. Reynolds number 120 is used by the controller when the actual Reynolds number is 100. This is a $+20\%$ error, and is maintained throughout the simulation so that, at every Reynolds number, the controller uses a Reynolds number that is 20% more than the actual. Fig. 10 shows the performance of the controller in the presence of this error. Again the controller exhibits very good robustness with respect to measurement error, reducing the drag compared to the open-loop case.

Remark 1. Previous studies on the effect of cylinder rotation on the structure of the wake behind the cylinder have shown that it is possible with appropriate cylinder rotation to influence the wake behind the cylinder (Taneda, 1977; Tokumaru & Dimotakis, 1991). For our problem, we have found that the proposed controller, using cylinder rotation, can prevent vortex formation up to Reynolds number 60. Fig. 11 illustrates the stabilizing effect of cylinder rotation. The top plot of the figure shows the flow field in the case of stationary cylinder at $Re = 60$, and the bottom plot of the figure shows the flow field at $Re = 60$ with the cylinder undergoing rota-

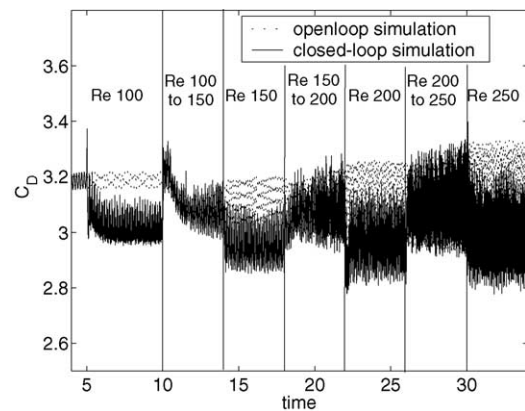


Fig. 10. Closed-loop simulation in the presence of measurement errors: C_D vs. time for Reynolds number varying from 100 to 250 under open-loop conditions (dashed line) and under closed-loop conditions in the presence of $+20\%$ measurement error (solid line).

tional oscillation, where wake stabilization (i.e., vortices are no longer formed) has been accomplished.

Remark 2. The underlying idea for the proposed control algorithm is based on stationary cylinder and open-loop rotational observations at various Reynolds numbers. Data from several stationary cylinder simulations revealed a linear relationship between the natural shedding frequency, f_{nat} , and the Reynolds number between $Re = 50$ – 500 . This linear relationship is shown in Fig. 5 of the paper. The open-loop rotational studies revealed that, at low Reynolds numbers, drag reduction is observed consistently when the cylinder is oscillated at $5f_{nat}$. The central idea behind the proposed control algorithm involved combining these two observations. Specifically, the controller has the following structure. The cylinder has a sensor that determines the incoming flow speed (or Reynolds number). Using the linear relationship between f_{nat} and Reynolds number shown in Fig. 5, the forcing frequency, f_f , of rotation was then set by the controller to be $5f_{nat}$ by changing the cylinder boundary conditions from no-slip to a sinusoidal, time-varying function with period $(1/5f_{nat})$.

Remark 3. Multiple control configurations have been applied to flow past the circular cylinder. Various types of actuation have been used in these control configurations, including

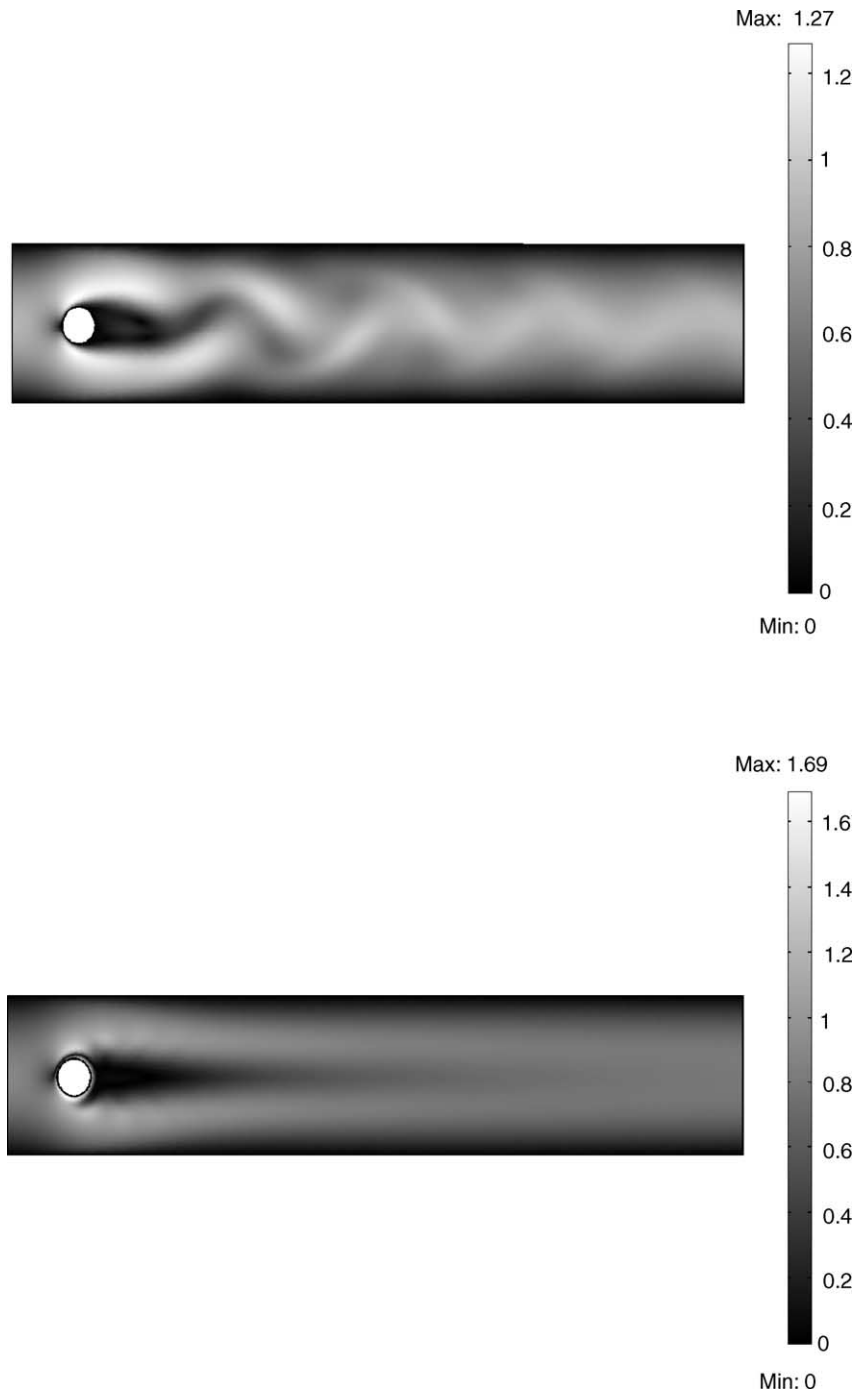


Fig. 11. Wake stabilization at $Re = 60$. Top plot: velocity field under stationary cylinder; bottom plot: velocity field under rotating cylinder based on the controller ($W = 3.2$ and $R_{fn} = 5$).

blowing and suction along the cylinder boundary, in-line oscillation, and transverse oscillation. For rotational oscillation, we have also implemented a few different controllers. In (Ray, 2003), a proportional (P) controller and a proportional-integral (PI) controller which adjusted the amplitude of cylinder rotational oscillation based on drag measurements taken along the cylinder boundary were implemented. It was found that the closed-loop feedback controller could not provide better performance than the open-loop controller for the same

range of Reynolds numbers. Additional details about these controllers can be found in (Ray, 2003). These controller designs, as well as controller designs based on reduced-order models which describe the dominant dynamics of this fluid dynamic system (Ray, 2003; see also, Christofides, 2001, for further results on feedback control of nonlinear PDEs), are limited by how much the cylinder can be actuated and how much this actuation ultimately affects the cylinder drag. Control schemes are also limited by the self-excited oscillations

that are inherent in the cylinder drag at this range of Reynolds numbers.

5. Conclusions

In this work, we focused on two-dimensional, incompressible viscous channel flow over an infinitely long cylinder and examined the effect of controlled rotational cylinder oscillation in reducing the drag exerted on the cylinder. Based on an analysis of the open-loop simulations, a control system was designed that automatically determines the frequency of cylinder oscillation, based on the Reynolds number, to consistently reduce the drag exerted on the cylinder for Reynolds numbers in the range 100–500.

Acknowledgement

Financial support for this work from the Wright-Patterson Air Force Base is gratefully acknowledged.

References

- Aamo, O. M., & Krstić, M. (2003). *Flow control by feedback*. London, UK: Springer-Verlag.
- Armaou, A., & Christofides, P. D. (2000a). Feedback control of the Kuramoto–Sivashinsky equation. *Physica D*, *137*, 49–61.
- Armaou, A., & Christofides, P. D. (2000b). Wave suppression by nonlinear finite-dimensional control. *Chemical Engineering Science*, *55*, 2627–2640.
- Baker, J., Armaou, A., & Christofides, P. D. (2000). Nonlinear control of incompressible fluid flow: application to Burgers' equation and 2D channel flow. *Journal of Mathematical Analysis & Applications*, *252*, 230–255.
- Baker, J., & Christofides, P. D. (2002). Drag reduction in transitional channel flow using distributed control. *International Journal of Control*, *75*, 1213–1218.
- Baker, J., Myatt, J., & Christofides, P. D. (2002). Drag reduction in flow over a flat plate using active feedback control. *Computers & Chemical Engineering*, *26*, 1095–1102.
- Batchelor, G. K. (1967). *An introduction to fluid dynamics*. Cambridge, UK: Cambridge University Press.
- Christofides, P. D. (2001). *Nonlinear and robust control of Partial Differential Equation Systems: Methods and applications to transport-reaction processes*. Boston, MA: Birkhauser.
- Christofides, P. D., & Armaou, A. (2000). Global stabilization of the Kuramoto–Sivashinsky equation via distributed output feedback control. *Systems & Control Letters*, *39*, 283–294.
- Gillies, E. A. (2001). Multiple sensor control of vortex shedding. *AIAA Journal*, *39*, 748–750.
- COMSOL Incorporated. (2001). FEMLAB: model library. Stockholm, Sweden: COMSOL.
- Juárez, H., Scott, R., Metcalfe, R., & Bagheri, B. (2000). Direct simulation of freely rotating cylinders in viscous flows by high-order finite element methods. *Computers & Fluids*, *29*, 547–582.
- Li, J., Chambarel, A., Donneaud, M., & Martin, R. (1991). Numerical study of laminar flow past one and two circular cylinders. *Computers & Fluids*, *19*, 155–170.
- Lu, X. Y., & Sato, J. (1996). A numerical study of flow past a rotationally oscillating circular cylinder. *Journal of Fluids and Structures*, *10*, 829–849.
- Papanastasiou, T. C., Malamataris, N., & Ellwood, K. (1992). A new outflow boundary condition. *International Journal of Numerical Methods in Fluids*, *14*, 587–608.
- Park, D. S., Ladd, D. M., & Hendricks, E. W. (1993). Feedback control of a global mode in spatially developing flows. *Physics Letters A*, *182*, 244–248.
- Protas, B., & Wesfreid, J. E. (2002). Drag force in the open-loop control of the cylinder wake in the laminar regime. *Physics in Fluids*, *14*, 810–826.
- Ray, P. (2003). *A study of drag force on a rotationally oscillating cylinder*. Master's Thesis. Los Angeles: University of California.
- Renardy, M. (1997). Imposing 'no' boundary condition at outflow: Why does it work?. *International Journal of Numerical Methods in Fluids*, *24*, 413–417.
- Roussopoulos, K. (1993). Feedback control of vortex shedding at low Reynolds numbers. *Journal of Fluid Mechanics*, *248*, 267–296.
- Schäfer, M., & Turek, S. (1996). Benchmark computations of laminar flow around a cylinder. *Notes on Numerical Fluid Mechanics: Flow Simulation with High Performance Computers II*, *52*, 547–566.
- Shiels, D., & Leonard, A. (2001). Investigation of a drag reduction on a circular cylinder in rotationally oscillation. *Journal of Fluid Mechanics*, *431*, 297–322.
- Singh, S. N., Myatt, J. H., Addington, G. A., Banda, S., & Hall, J. K. (2001). Optimal feedback control of vortex shedding using proper orthogonal decomposition models. *Journal of Fluid Engineering, Transactions of ASME*, *123*, 612–618.
- Taneda, S. (1977). Visual study of separated flows around bodies. *Progress in Aerospace Science*, *17*, 287–348.
- Tokumaru, D. T., & Dimotakis, P. E. (1991). Rotary oscillation control of a cylinder wake. *Journal of Fluid Mechanics*, *224*, 77–90.
- Williamson, C. H. K. (1988). Defining a universal and continuous Strouhal–Reynolds number relationship for the laminar vortex shedding of a circular cylinder. *Physics in Fluids*, *31*, 2742–2744.
- Williamson, C. H. K. (1996). Vortex dynamics in the cylinder wake. *Annual Review in Fluid Mechanism*, *28*, 477–539.